THE ASTROPHYSICAL JOURNAL, 413:281–292, 1993 August 10

BATSE OBSERVATIONS OF GAMMA-RAY BURST SPECTRA. I. SPECTRAL DIVERSITY

D. BAND, J. MATTESON, AND L. FORD
Center for Astrophysics and Space Sciences 0111, University of California at San Diego, La Jolla, CA 92093
B. SCHAEFER, D. PALMER, B. TEEGARDEN, AND T. CLINE
NASA/Goddard Space Flight Center, Code 661, Greenbelt, MD 20771
M. BRIGGS, W. PACIESAS, AND G. PENDLETON
University of Alabama at Huntsville, Huntsville, AL 35899
G. FISHMAN, C. KOUVELIOTOU, C. MEEGAN, AND R. WILSON
NASA/Marshall Space Flight Center, ES-62, Huntsville, AL 35812
AND
P. LESTRADE
Mississippi State University, P.O. Box 5167, Mississippi State, MS 39762
Received 1992 November 17; accepted 1993 February 19

ABSTRACT

We studied the time-averaged gamma-ray burst spectra accumulated by the spectroscopy detectors of the Burst and Transient Source Experiment (BATSE). The spectra are described well at low energy by a power-law continuum with an exponential cutoff, $N_E(E) \propto E^{\alpha} \exp(-E/E_0)$, and by a steeper power law, $N_E(E) \propto E^{\beta}$ with $\alpha > \beta$, at high energy. However, the spectral parameters α, β, and E_0 vary from burst to burst with no universal values. The break in the spectrum, E_0, ranges from below 100 keV to more than 1 MeV, but peaks below 200 keV with only a small fraction of the spectra breaking above 400 keV. Consequently, it is unlikely that a majority of the burst spectra are shaped directly by pair processes, unless bursts originate from a broad redshift range. We find that the correlations among burst parameters do not fulfill the predictions of the cosmological models of burst origin, but our burst sample may not be appropriate for such a test. No correlations with burst morphology or the spatial distribution were found. We also studied the process of fitting the BATSE spectral data. For example, we demonstrate the importance of using a complete spectral description even if a partial description (e.g., a model without a high-energy tail) is statistically satisfactory.

Subject headings: gamma rays: bursts — radiation mechanisms: miscellaneous

1. INTRODUCTION

The statistics of gamma-ray bursts have recently accentuated the mystery of burst origin: burst isotropy and the paucity of weak bursts observed by the Burst and Transient Source Experiment (BATSE) on the *Compton Gamma Ray Observatory* (*GRO*) (Meegan et al. 1992) refute the local neutron star paradigm and lead to extended Galactic halo or cosmological source models. The detailed properties of each burst, such as time history or spectra, reflect fundamental aspects of the burst phenomenon which must be explained by the new burst theories. In particular, burst spectra are among their more perplexing characteristics: somehow the burst source emits the bulk of the radiated energy in the gamma-ray band of ~0.1–1 MeV. The gamma-ray spectrum may provide crucial diagnostics of the underlying physical processes within a burst, and may be a discriminant between different emission mechanisms.

This is the first in a series of studies of the gamma-ray burst spectra accumulated by BATSE's spectroscopy detectors (SDs). In the current study we investigate spectra averaged over entire bursts and search for global properties, such as whether spectra can be described by a universal shape, as well as correlations with other burst properties, such as hardness with burst fluence. In future studies we will investigate other properties, such as the evolution of the spectrum during a given burst. Observations by other detectors (e.g., Norris et al. 1986) and preliminary results from the SDs (Band et al. 1992) show that the spectral shape and hardness change significantly during a typical burst. The spectra studied here are averages over widely varying instantaneous spectra, and thus reflect not only the physical processes operating at any given moment but also the temporal evolution of the burst (weighted, of course, by the count number).

The characterization of burst spectra has evolved over time as instruments have become more sensitive and more bursts have been analyzed. Cline et al. (1973) and Cline & Desai (1975) found that the *IMP 6* and *IMP 7* spectra, which consisted of 14 channels from ~60 keV to ~1 MeV, were consistent with $N_E(E) \propto \exp(-E/E_0)$ photons cm^{-2} keV^{-1}, where $E_0 =$ 150 keV. The *IMP 7* spectra also showed a high-energy power law with spectral index -2.5 tangent to the exponential. Mazets et al. (1982) described the spectra from 143 bursts observed by Konus on *Venera 11* and *12* as $N_E(E) \propto E^{-1} \exp(-E/E_0)$; the Konus spectra covered the energy range 30 keV–2 MeV in 16 channels. The E_0 distribution ranged from ~20 keV to ~2 MeV, peaking at 250 keV. Low-energy deviations from this spectral form were interpreted as resulting from cyclotron absorption, and not as an intrinsically flatter continuum. The *Solar Maximum Mission* (*SMM*) detected emission above 1 MeV in excess of an extrapolation of the low-energy spectrum (Matz et al. 1985). Most recently, two instruments on *GRO* observed a high-energy tail from 1B 910503: up to ~10 MeV for COMPTEL (Winkler et al. 1992) and ~100 MeV for EGRET (Schneid et al. 1992). Thus burst spectra typically have been described as $N_E \propto E^{\alpha} \exp(-E/E_0)$ (Barat et al. 1984), flattening out smoothly to $N_E \propto E^{\beta}$, with $0 > \alpha > \beta$ (Hurley 1989; Higdon & Lingenfelter 1990). We find

that the BATSE spectra are well described by this spectral form, but that α, β, and E_0 all vary; there are no universal values. Such diversity must be addressed by physical models of the burst process.

While bursts show a great deal of diversity, few correlations have been found among the different burst properties. Such correlations would provide a deeper understanding of the underlying physical processes, and they might permit the identification of burst classes with different energy release and emission mechanisms. The systematic description of a large burst sample adds an additional dimension for classification schemes. Unfortunately, while we do find some new correlations, we do not find any striking characteristics upon which to base a classification taxonomy.

A central aspect of this study, and of those which follow in this series, is the fitting of model spectra to the observed count spectra. We therefore need to understand the consequences of the functional forms used, and of the analysis methods employed. For example, the signal-to-noise ratio (S/N) varies with energy as a result of the intrinsic spectrum, the background, and the detector efficiency. Consequently, the spectrum is not well determined at high energies, and many spectra can be fitted adequately by a model that cuts off exponentially. However, other instruments and BATSE spectra with sufficient counts show that there is usually a high-energy tail. As we will show, omitting this high-energy component hardens the low-energy component. To better understand the nature of the fits, we have simulated the creation and fitting of BATSE spectra.

Before presenting the analysis of burst spectra, we describe the SDs, the method of analyzing this data, and the spectra used in this study (§ 2). To better understand the analysis methodology, we study the spectral fitting of SD spectra (§ 3). In § 4 we present a quantitative description of burst spectra and investigate the relationships between various quantities. Finally, in § 5 we draw conclusions from these results.

2. METHODOLOGY

2.1. *Instrumental Summary*

BATSE consists of eight modules at the corners of the *GRO* spacecraft. Each module contains two detectors: a large-area detector (LAD), whose purpose is the detection of transient gamma-ray events and the observation of their time histories; and an SD dedicated to spectra. In addition, the LADs have been very successful in monitoring sources through Earth occultations and folding the count rate at known periods. Although the LADs also provide spectra, here we present results from the SDs, since they have superior spectral resolution and are sensitive over a broader energy range. Each SD detector is built around a 5″ diameter by 3″ thick NaI(Tl) crystal. These crystal dimensions give the SDs a fractional energy resolution of $\sim$7% FWHM at 662 keV, with an $\sim E^{-0.4}$ dependence. A 3″ diameter beryllium window in the front face of each aluminum detector housing increases the detector response down to $\sim$5 keV for face-on bursts. The energy that a photon deposits in the crystal is first analyzed into 2782 linear pulse-height channels, which are then compressed into 256 pseudologarithmic channels. Most of these compressed channels are finer than the detectors' energy resolution, particularly for the spectra used in this study. The photomultiplier gain and the electronic low-energy threshold can be adjusted to shift the analyzed energy band over a wide range. When a detector is operated at a higher gain, it is sensitive over a lower energy range. The BATSE detectors are described by Fishman et al. (1989a); Fishman et al. (1989b) discuss their scientific capabilities; and the calculation of the detector response is outlined by Pendleton et al. (1989).

After a burst is detected by the LADs, BATSE collects a prodigious quantity of data during a $\sim$4 minute burst mode. One of the resulting data products, known by the mnemonic SHERB ("SD" plus "high-energy resolution" plus "burst") is a series of 192 spectra from the four SDs with the highest count rates, with more frequent accumulations for the more brightly illuminated detectors. A time-to-spill criterion determines the accumulation time in multiples of 0.064 s with a minimum of 0.128 s. Since there is no way of predicting the burst duration a priori, the SHERB almost always either continues past a burst (and may consist predominantly of background) or finishes before the end of a long and strong burst. Since the purpose of the current study is to analyze the spectra of entire bursts, we averaged all the SD spectra over the duration of each burst. If the SHERB ended before the burst, we used the available spectra as noted in Table 1, where all bursts used in this study are recorded. Since bursts often evolve from hard to soft (Norris et al. 1986; Band et al. 1992), the loss of the end of a burst may harden the resulting observed spectrum.

2.2. *Burst Analysis*

Since BATSE provides spectra from the four most brightly illuminated detectors for each burst (although some of the detectors are at an angle greater than 90° to the burst), we chose for each burst in our sample the average spectrum with the best statistics which extends down to $\sim$30 keV or below. We only considered spectra that at least covered the energy range 30–100 keV to constrain the low-energy spectral softening (as demonstrated below). Over the course of the mission a progressively larger fraction of the detectors has been set at high gain, lowering the usable energy range. Therefore, the choice of spectra for a given burst has increased since *GRO*'s launch.

Each spectrum was fitted over the largest energy range possible. The actual energy range depended on the detector's gain and electronic cutoff; an electronic artifact in the lowest few channels above the electronic cutoff makes these channels unusable (Band et al. 1993a). Thus the low end of the spectrum, E_1 ranged between 10 and 30 keV, while the high end, E_2, varied from 1200 to 3000 keV; the energy range for each burst is presented in Table 1. To provide a measure of the energy range which is well determined, we also list $E_{3\sigma}$ of the highest energy channel with a signal-to-noise ratio per channel greater than 3. Since $E_{3\sigma}$ is defined at the lower end of a channel while E_2 is defined at the upper end of a channel, $E_{3\sigma} < E_2$, even for spectra with a large S/N in the highest channel. As we show in § 3, the spectrum above $E_{3\sigma}$ continues to influence the fit: the correct spectral parameters are found on average, but the dispersion around the true values increases as the S/N decreases.

The spectra were analyzed using the Burst Spectral Analysis Software (BSAS) package (Schaefer 1991). The basic fitting algorithm is based on CURFIT of Bevington (1969, p. 237), which finds the optimum spectral parameters by minimizing χ^2. In our case χ^2 minimization is justified because the number of counts in most channels is large enough to approximate a Poisson distribution with a Gaussian. In addition, χ^2 can be used when at least 80% of the data bins have more than five events (Eadie et al. 1971, p. 257). While the upper energy channels are compressed aboard *GRO* so that the channels in the

TABLE 1

BURSTS ANALYZED

Burst[a]	Detector	E_1[b] (keV)	$E_{3\sigma}$[c] (keV)	E_2[d] (keV)	Duration[e] (s)	Class[f]
1B 910430	6	30.7	714.8	3098.4	40.192[g]	C
1B 910502	0	20.4	1233.8	2983.4	6.592	C
1B 910503	6	30.8	2545.9	3105.1	9.472[h]	C
1B 910507	1	30.5	514.8	3704.1	20.416	C
1B 910511	7	31.6	210.3	2808.7	2.432	C
1B 910523	6	30.4	130.6	3062.8	2.432[h]	C
1B 910601	0	10.1	1624.2	3136.6	9.408[g]	C
1B 910627	6	30.8	363.2	3353.4	20.160	C
1B 910629	0	25.7	509.6	3187.8	8.832	S
1B 910630	6	36.2	571.4	3378.1	18.880	S
1B 910709	0	26.0	166.8	3496.7	0.960	S
1B 910803	7	30.5	337.1	3090.1	19.712	C
1B 910809	0	25.6	619.2	3176.9	10.688	C
1B 910814C	3	10.1	643.5	2713.8	78.080	C
1B 910814B	6	35.8	1994.5	3583.6	69.632	S
1B 910905	0	25.1	3383.3	3509.8	77.056	C
1B 910930	0	26.0	189.7	3216.9	24.960	C
1B 911016	0	15.5	161.4	1595.5	14.400[h]	C
1B 911031	3	15.0	911.6	1501.6	34.688	C
1B 911104	3	10.2	669.9	1518.9	7.744	C
1B 911106	4	20.1	859.5	1693.3	19.840	C
1B 911109	4	20.2	419.6	1698.6	5.504	C
1B 911118	4	20.8	1144.4	1897.5	16.576	C
1B 911123	7	16.4	142.3	1873.1	5.760	C
1B 911126	4	20.2	1101.0	1825.0	57.472	C
1B 911127	1	30.9	859.1	3279.5	26.368	C
1B 911202	7	20.2	1405.7	1790.0	23.040	C
1B 911209	1	30.6	759.7	3147.4	24.320[i]	C
1B 911210	1	30.6	227.8	3145.5	4.352	S
1B 911217	1	20.6	273.6	2152.3	4.736	C
1B 911227	3	15.4	906.4	1856.5	25.216[i]	C
1B 920110	6	30.6	645.3	4345.9	70.464[g]	C
1B 920130	4	20.1	171.8	1691.4	77.824	C
1B 920210	4	15.4	844.6	1250.1	49.984	C
1B 920221	7	10.2	606.1	1376.5	12.544	C
1B 920226	7	10.2	1329.3	1378.7	29.120	C
1B 920227	6	15.2	175.2	1280.6	1.024	C
1B 920227B	7	10.4	483.3	1399.5	37.952	C
920307_01086	1	20.9	316.7	1606.8	16.320	S
920308_17747	0	15.1	1161.2	1267.4	27.200	C
920311_08426	5	10.3	1243.9	1290.3	28.864	C
920315_15569	1	36.0	935.6	3571.0	24.896	C
920320_44340	5	10.1	1081.9	1319.2	45.440	C
920325_62257	1	30.0	618.1	3613.9	37.632	C
920331_65750	5	10.2	318.6	1283.0	128.704	C
920404_47506	0	15.1	1039.9	1267.3	6.400	S
920406_09855	2	25.5	1135.8	1177.6	29.952[g]	C
920502_62802	5	10.2	394.4	1283.0	23.040	C
920511_23247	1	30.4	537.6	2851.7	81.216	C
920513_60781	7	10.0	1110.4	1278.2	43.328[g]	C
920517_11876	7	10.2	787.3	1297.8	8.832[g]	S
920524_13904	2	19.5	677.8	1257.3	60.032[g]	C
920525_12423	5	10.0	1300.6	1349.2	26.048	C
920530_82797	2	20.1	1114.9	1281.8	8.192	S

[a] Bursts before the end of 1992 February are identified according to the First BATSE Burst Catalog (Fishman et al. 1993). Subsequent bursts are identified by the date and time (in seconds) of their occurrence.
[b] Low-energy edge of lowest channel included in spectrum.
[c] Energy at the bottom of the highest channel with S/N $\geq$ 3.
[d] High-energy edge of highest channel included in spectrum.
[e] Accumulation time of spectrum.
[f] Morphological class: C = complex, multipeaked; S = single peak.
[g] Spectral data end in middle of burst.
[h] Spectral data include first of two major spikes.
[i] Spectral data do not include weak features after major part of burst.

data returned to Earth are spaced pseudo-logarithmically, we further rebinned the data to make the channels used for the fits more nearly logarithmic. Consequently, the spectra we fit generally contained $\sim$100 channels. An example of a burst spectrum with a model fit is shown in Figure 1.

In parallel with this study of burst spectra, we have been improving the analysis software and developing a deeper understanding of the detectors. Consequently, the results presented here are not final fits to the burst spectra. The detector response used in these fits included the direct and spacecraft-scattered photons (Pendleton et al. 1989) but not the radiation scattered off the Earth. A detailed model of the BATSE module and a simplified spacecraft description were used to calculate the scattering in the detector environment. Earth scatter should be important in only a few spectra from detectors with a large burst-detector normal angle and for which the Earth fills a large portion of the observable sky. The channel-energy calibration utilized in forming the spectra used in this study has since been improved, particularly at low energy. The calibration used here could be off by up to $\sim$5 keV at $\sim$30 keV. From a few comparisons we find quantitative differences between the parameter values found from fitting the same spectrum calibrated by the two methodologies; these differences do not affect our conclusions. Future spectral analysis will use the improved calibration; this calibration methodology also removes the instrumental feature just above the low-energy electronic cutoff (Band et al. 1993a).

The background spectra subtracted from the observed burst spectra were interpolated from observed background spectra accumulated $\sim$1000–2000 s before and after the burst. If the SHERB accumulations continued past the end of the burst, the background SHERB spectra were also used. The background at the time of the burst was calculated from a channel-by-channel cubic fit in time. Occasionally a lower order fit was used if only a small number of background spectra were available or if the cubic fit did not appear justified because the background varied slowly. As judged by the relative size of the uncertainties and the channel-to-channel variations, the calculated background spectra were acceptable for the bursts in the sample; a number of bursts were not included in the sample because of difficulties in calculating a reasonable background spectrum.

Based on the previous work described in § 1, we character-

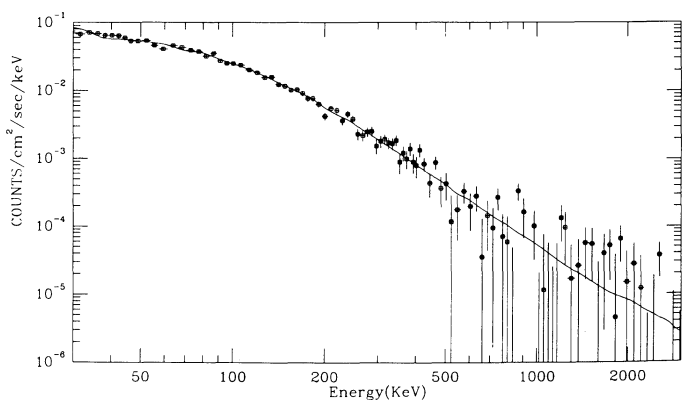

FIG. 1.—Example of a spectral fit. The GRB model (eq. [1]) was fitted to the average spectrum of 1B 911127. The low-energy spectral index is $\alpha = -0.968 \pm 0.022$, the high-energy spectral index $\beta = -2.427 \pm 0.07$, and the break energy $E_0 = 149.5 \pm 2.1$. With 100 degrees of freedom, $\chi^2 = 121.58$.

ized the background-subtracted continuum by the functional form

$$N_E(E) = A\left(\frac{E}{100\text{ keV}}\right)^{\alpha}\exp\left(-\frac{E}{E_0}\right), \quad (\alpha-\beta)E_0 \geq E,$$

$$= A\left[\frac{(\alpha-\beta)E_0}{100\text{ keV}}\right]^{\alpha-\beta}\exp(\beta-\alpha)\left(\frac{E}{100\text{ keV}}\right)^{\beta}, \quad (\alpha-\beta)E_0 \leq E, \quad (1)$$

which we call the GRB model. This model was constructed so that it and its derivative are continuous. This functional form reproduces the common description of burst continuum with $\alpha \sim -1$ and $\beta \sim -2$. In addition, many standard spectral shapes can be represented by this model: single power law ($E_0 = \infty$), photon exponential ($\alpha = 0$, $\beta = -\infty$), and energy exponential (often referred to as optically thin thermal bremsstrahlung without the Gaunt factor: $\alpha = -1$, $\beta = -\infty$). We stress that we use this functional form as a characterization of the spectrum without implying any direct relation to the underlying physical processes. For example, although E_0 plays the role of the temperature in thermal spectral forms and is therefore often called the "temperature." it probably does not correspond to a physical temperature, since bursts are unlikely to involve thermal processes (Harding 1991).

In general the fits are statistically acceptable, since the reduced χ^2 is usually of order unity for $\sim$100 degrees of freedom (see the more detailed discussion in § 4), although this can be misleading, as we show in § 3. We estimate the 1 σ uncertainties assuming one parameter of interest and holding all other parameters fixed at their best-fit values. These estimates are more accurate than the uncertainties usually provided by the CURFIT routine (Schaffer 1991) but are not as accurate as those derived from exploring the χ^2 surface fully.

For each burst we present fits to spectra from only one detector, thus avoiding the difficulty of relative energy and flux calibration. We have performed joint fits from multiple detectors and find the results are generally consistent with the fits to single detectors as long as a high-gain detector, which is sensitive at low energy, is included in the joint fit: the flat low-energy (25–100 keV) portion of the spectrum determines the value of α in the GRB model.

2.3. *Characterization of Burst Sample*

Our sample of 54 bursts, listed in Table 1, comprises almost all the strong bursts until the end of 1992 May. Chosen for spectral analysis were those bursts for which the peak count rate summed over all the triggered LADs and accumulated in 0.064 time bins exceeded $\sim$10,000 counts s^{-1} above background. The count-rate criterion was not applied rigidly, since a number of weaker events with interesting time histories were included. In addition, a few strong bursts were not included because of data processing difficulties such as missing data or a poor background spectrum. Finally, in this study we used only SHERB data, which often misses most of the counts from extremely short duration bursts. Thus we do not include in our sample the bursts which consist of very short spikes. Since the selection criteria were not applied uniformly, the sample is not rigorously statistically complete, but it is most probably effectively so.

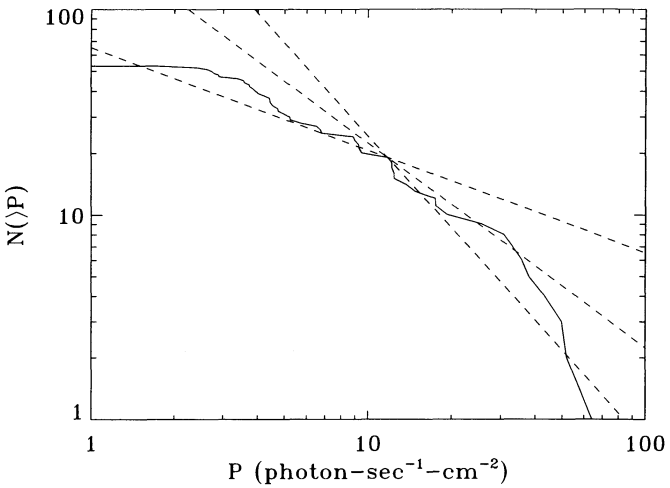

FIG. 2.—$N(>P)$ vs. P for the burst sample, where P is the peak photon number flux. The dashed curves show $P^{-1/2}$, P^{-1}, and $P^{-3/2}$ dependences.

Given that the bursts in our sample constitute the bright end of the BATSE distribution, are these bursts still in the homogeneous part of the spatial distribution, or do they sample the region where the source density decreases? Figure 2 presents the distribution of bursts by peak flux P (i.e., photons s^{-1} cm^{-2}) averaged over 0.064 s bins; as can be seen, over a decade in P the number is distributed as $P^{-0.8}$, which is typical of the entire statistically complete BATSE data base as opposed to the $P^{-3/2}$ dependence expected of a homogeneous distribution. Thus our sample probably samples bursts out to distances where the source distribution is inhomogeneous.

The bursts are spread uniformly across the sky. Table 2 summarizes their spatial distribution in both Galactic and equatorial coordinates. In addition, 24 of the 54 bursts are found within 30° of the Galactic plane (i.e., $|b| < 30°$); on average, half the sources will be within $|b| < 30°$ for an isotropic distribution.

No consistent burst taxonomy has been developed and accepted for gamma-ray bursts. However, for the purpose of categorizing the bursts observed by BATSE, the BATSE instrument team uses a simple scheme based on time-history morphology (Kouveliotou et al. 1992) similar to the classification proposed by Barat et al. (1981). As listed in Table 1, of the 54 bursts in our sample, 45 are classified as complex, multi-peaked events and nine consist of a single pulse with no evident substructure; as described above, the SHERB data type used for this study is not appropriate for studying very short bursts. Thus, our sample does not contain enough bursts in the different morphological classes for us to draw firm conclusions concerning differences between these classes.

TABLE 2

SPATIAL DISTRIBUTION OF BURST SAMPLE

	R.A.			l	
DECL.	<180°	>180°	b	<180°	>180°
>0°	14	14	>0°	17	12
<0°	11	15	<0°	12	13

3. DATA ANALYSIS ISSUES

In order to understand the peculiarities and sensitivities of the spectral data and the biases which may affect the spectral analysis in this and future studies, we ran simulations in which we created and then fitted model SD spectra. We used the simulations to understand the trends with signal-to-noise ratio, the correlations between parameters, and the implications of modeling a spectrum with an overly simplistic spectral form.

In these simulations we first created a simulated count spectrum, which we then fitted with spectral models using CURFIT (Bevington 1969, p. 237). As the underlying signal spectrum, we used the GRB spectral form in equation (1), both with and without the high-energy tail (i.e., the E^{β} power law); these will be referred to as the four- and three-parameter GRB models, respectively. Simulated count spectra were created by multiplying the signal spectrum by a simplified detector response which only includes an approximation to the SD efficiency. Gaussian noise was then added to approximate counting statistics; that the noise was Gaussian justifies χ^2 minimization in CURFIT. We also considered the effects of an underlying background spectrum B_i on the counting statistics. Based on observed background spectra, $B(E) = 0.02(E/100\ \mathrm{keV})^{-1.5}$ counts cm^{-2} s^{-1} was used (actually the background is not a flux, but it can be expressed as such for comparison with the count rate). Our simulations covered the energy range 30–3000 keV in 100 logarithmically spaced channels. For the simulations presented here we used $\alpha = -0.5$, $E_0 = 300$ keV, $\beta = -2$ (for the four-parameter models) and an integration time of 1 s.

We created a large set of simulated count spectra (typically 1000) with the same signal spectrum, duration, and background spectrum (if a background was included) and considered the distribution of fit parameters. Table 3 describes a series of relevant simulations. For each parameter x, Table 3 provides the value used for the signal spectrum x^0, the median (not the mean) fit value x_{fit}, and the dispersion $\sigma_x = [\langle (x - x_{\mathrm{fit}})^2 \rangle]^{1/2}$. Also given are the reduced χ^2, χ^2/ν (where ν is the number of degrees of freedom), and the maximum S/N in any channel.

When we fit the simulated spectra with the same functional form as was used to create the signal spectra (e.g., the four-parameter GRB model with the four-parameter model), we found that the median value of each parameter reproduced its "true" value to within a few percent. As expected, the average $\chi^2/\nu \simeq 1$. However, when the three-parameter GRB model was fitted to spectra created from the four-parameter model (i.e., we left the high-energy power law out of the models fitted to the simulated spectra), the median parameter values were systematically biased regardless of the S/N. We found that four-parameter GRB models created with $\alpha = -0.5$ and $E_0 = 300$ keV were best fitted by three-parameter models with median values of $\alpha' \sim -0.7$ and $E_0' \sim 480$ keV. The three-parameter model apparently attempts to fit the high-energy power law of the four-parameter model by shifting the exponential cutoff to higher energy and softening the low-energy power-law component. The average χ^2/ν was significantly larger than unity when the S/N was high but dropped to unity as the S/N decreased below ~ 5.

As the S/N decreases, the width of the distribution of fitted parameters increases, while the median parameter values change little if at all. Nonetheless, all the simulated spectra can be modeled by the original signal spectrum (i.e., with the same set of spectral parameters) with a χ^2 only slightly larger than the minimum value. In our simulations we find a difference in χ^2/ν of ~ 0.04 between the signal and best-fit spectra. We conclude that in fitting an observed spectrum, a correct hypothesis will not be rejected even if the best-fit parameters differ from the "true" parameters of the hypothesis.

The parameters fitted to a series of simulated spectra based on the same underlying signal spectrum were correlated. Thus we find that the fits fall in a thin crescent-shaped region of (α, E_0)-space whose size increases as the S/N decreases. The correlation results from S/N variations across the spectrum. The S/N peaks in the middle of the spectrum as a result of the decreasing effective area at the low end of the spectrum, and

TABLE 3

FITS TO SIMULATED SPECTRA

n^0	n_{fit}	σ_n	α^0	α_{fit}	σ_α	β^0	β_{fit}	σ_β	E_0^0	$E_{0\,\mathrm{fit}}$	σ_{E_0}	χ^2/ν	S/N
Four-Parameter Fit to Four-Parameter Model; No Background													
0.3	0.3001	0.1346	−0.5	−0.4992	0.05093	−2	−2.001	0.05795	300	299.5	29.12	0.9959	10.67
0.1	0.1003	0.007756	−0.5	−0.4943	0.08179	−2	−2.002	0.09335	300	298.1	46.79	1.0128	6.16
0.05	0.05018	0.005692	−0.5	−0.4996	0.1182	−2	−2.007	0.1242	300	298.5	66.20	1.0030	4.35
0.02	0.02026	0.004329	−0.5	−0.4820	0.1930	−2	−2.011	0.2481	300	291.8	99.95	1.0026	2.75
0.0075	0.007703	0.002967	−0.5	−0.4555	0.2983	−2	−2.020	0.4515	300	284.8	161.8	1.0061	1.69
Four-Parameter Fit to Four-Parameter Model; with Background													
1.0	1.001	0.02545	−0.5	−0.4986	0.02811	−2	−2.001	0.03477	300	299.6	16.42	1.0014	19.20
0.3	0.3006	0.01438	−0.5	−0.4982	0.05420	−2	−2.001	0.06544	300	299.0	30.25	1.0022	10.20
0.1	0.1000	0.009025	−0.5	−0.5015	0.09998	−2	−2.002	0.1256	300	300.1	56.67	1.0057	5.45
0.06	0.06004	0.007989	−0.5	−0.4978	0.1425	−2	−2.008	0.1707	300	300.1	77.45	1.0010	3.95
0.03	0.03048	0.009331	−0.5	−0.4726	0.2480	−2	−2.014	0.3522	300	289.8	142.1	1.0064	2.45
Three-Parameter Fit to Four-Parameter Model; No Background													
1.0	0.8385	0.01408	−0.5	−0.6973	0.02092	−2	...	...	300	485.5	23.23	3.1510	19.48
0.3	0.2528	0.07530	−0.5	−0.6920	0.03859	−2	...	...	300	478.7	43.01	1.6430	10.67
0.1	0.08396	0.004467	−0.5	−0.6926	0.06488	−2	...	...	300	484.0	75.13	1.2072	6.16
0.04	0.03380	0.002735	−0.5	−0.6925	0.1011	−2	...	...	300	479.3	120.7	1.0827	3.90
0.005	0.004256	0.001244	−0.5	−0.6620	0.3008	−2	...	...	300	455.0	724.7	1.0075	1.38

the falling number of counts as well as the diminishing detector efficiency at the high end. The energy of the maximum S/N depends on the hardness of the signal and its strength relative to the background; the S/N peaked at ~120 keV in our simulations. As the overall S/N drops, a smaller range of the spectrum is well determined. Fits to the spectra will go through this well-determined segment, and will have the same slope as the signal spectrum, while outside this energy range statistical fluctuations cause the simulated spectrum to deviate from the "true" spectrum. Thus if E_r is the energy of the peak of the S/N, we expect that all fitted spectra and their derivatives will be the same at E_r. In general E_r will be in the low-energy component of the GRB spectral form. From the assumption that the model derivative is always the same at E_r, we find that $\alpha'/E_r + 1/E_0'$ is constant, where α' and E_0' are the quantities from the fit. This predicts that the fit values of α' and $1/E_0'$ should be linearly anticorrelated. Indeed, linear regressions to α' and $1/E_0'$ from simulations based on a common signal spectrum give correlation coefficients of $r \sim 0.94$; Figure 3 demonstrates this linear anticorrelation. This figure also shows the bias resulting from fitting a three-parameter model to a four-parameter spectrum.

The results of these simulations provide a great deal of insight into fitting gamma-ray burst spectra. First, we see that on average the fit finds the correct parameters regardless of the S/N if the appropriate model is fitted to the observed spectrum. Thus channels with very small S/N continue to influence the fit and should not be neglected. Often the high-energy part of the spectrum consists predominantly of upper limits; we see that the fitted spectrum should not be truncated.

Second, the dispersion of the fitted parameters around the average values increases as the S/N decreases. Any given fit may result in parameters that differ significantly from the true values. However, the χ^2 for the correct parameters is only a little larger than the minimum χ^2. Thus, if there is a universal spectral shape, then fits with the appropriate parameters fixed at their universal values should be acceptable. The deviations of the parameters are correlated in such a way that the fit tracks the true spectrum in the energy range with the highest S/N.

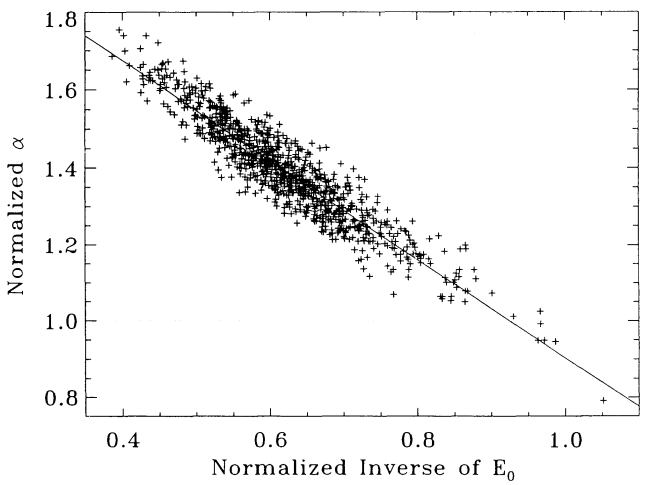

FIG. 3.—Distribution of α and the inverse of E_0 from the fit of $N_E = n(E/100)^{\alpha} \exp(-E/E_0)$ to 1000 simulated spectra created with $N_E = 0.1(E/100)^{-0.5} \exp(-E/300)$ for $E < 450$, and $N_E = 2.13 \times 10^3 E^{-2}$ for $E \geq 450$. No background spectrum was used. The fitted value of α was normalized by $\alpha = -0.5$, while E_0 was normalized by $E_0 = 300$ keV; thus at (1, 1) the fit found the input parameters. The resulting count spectra had peak signal-to-noise values of 7.5. The solid line shows a linear fit ($r = -0.933$) to the pairs of fit parameters.

Third, fitting a spectrum created with a high-energy tail (the four-parameter GRB model) with a model without such a tail (the three-parameter model) biases the fitted parameters toward harder values. The resulting fits to simulated spectra with large S/N are mediocre as measured by a large χ^2/ν. Yet, as the S/N decreases, so does χ^2/ν. Consequently, the simpler three-parameter model can appear adequate statistically yet will be clearly biased toward harder parameters. We know from both *SMM* (Matz et al. 1985) and *GRO* (Schneid et al. 1992; Winkler et al. 1992; and results below) observations that the time-averaged spectra of sufficiently strong bursts have a high-energy power-law tail with $\beta \sim -2$. The fit to a given burst spectrum with low S/N may not require such a tail, yet omitting this component produces clearly incorrect results. This is indeed seen in fitting burst spectra accumulated over short burst time segments: a high-energy tail may be required to fit the spectrum of an entire burst composed of many SHERB spectra, but may not be required to fit individual SHERB spectra, each with a much reduced S/N. Of course, we are unable to prove that the high-energy tail is present throughout the burst. Nonetheless, we should use the prior information and include the high-energy tail in the fit.

4. RESULTS

4.1. *Average Spectral Shape*

We find that for the SD's spectral resolution, all burst spectra can be characterized by the same simple four-parameter form presented in equation (1). However, there is not a common set of burst parameters, and α, β, and E_0 must all be permitted to vary. Thus canonical parameter values mentioned in the past—$\alpha = -1$ or $\alpha = 0$, $\beta = -2$, and $E_0 = 150$ keV—are not universal. In general, the continuum gives the impression of continuous curvature below a few hundred keV which our GRB functional form is able to approximate over the observed energy range with good statistics. Perhaps in the future our four-parameter model will be inadequate to describe spectra observed by detectors with better spectral resolution.

To demonstrate that bursts cannot be described by a universal spectrum, we compared fits of our sample's 54 burst spectra by models where $\alpha = -1$ and $\beta = -2$ to fits with all four parameters free to vary. In this section we refer to GRB models with $\alpha = -1$ and $\beta = -2$ as two-parameter models, and those with all four parameters free to vary as four-parameter models. The resulting parameters are listed in Table 4. Note that $E_{0,2}$ and $E_{0,4}$ were found using the two- and four-parameter models, respectively. Using the F-test (Martin 1971, pp. 146–147; Briggs 1991, p. 227), we tested whether allowing α and β to vary was statistically required. Table 4 gives the significance: the probability of the difference in χ^2 between the two- and four-parameter models if the two-parameter model is indeed correct. Consequently, a large value of the significance indicates that the two-parameter model (i.e., $\alpha = -1$ and $\beta = -2$) is an acceptable description, while a small value requires α and β to be free. The histogram in Figure 4 shows that the significance is small for a large fraction of the bursts.

Figure 4 also presents the significance distribution by the low-energy cutoff E_1 of the fitted spectrum. It is apparent that spectra which begin at a lower energy are more likely to

TABLE 4

FITS TO GAMMA-RAY BURST SPECTRA

Burst	Significance[a]	$E_{0,2}$[b]	$E_{0,4}$[c]	α[d]	β[e]	χ^2_4/ν[f]
1B 910430	8.312×10^{-8}	161.4 ± 3.9	312.5 ± 10.8	−1.211 ± 0.029	−5.000[g]	138.90/102
1B 910502	2.430×10^{-14}	15.5 ± 0.2	14.8 ± 0.2	−1.201 ± 0.007	−2.156 ± 0.008	126.31/107
1B 910503	4.861×10^{-20}	696.3 ± 8.8	349.7 ± 2.7	−0.668 ± 0.007	−2.145 ± 0.027	192.28/102
1B 910507	3.797×10^{-9}	190.7 ± 8.8	71.9 ± 1.2	0.200 ± 0.068	−4.326 ± 1.036	132.85/108
1B 910511	0.6767	160.9 ± 11.5	102.3 + 5.9	−0.743 ± 0.121	−1.893 ± 0.094	105.87/100
1B 910523	3.546×10^{-3}	24.6 ± 2.8	48.7 ± 2.9	−0.423 ± 0.165	−5.000	313.13/102
1B 910601	9.878×10^{-16}	415.5 ± 6.2	599.9 ± 13.5	−1.042 ± 0.014	−5.000	245.60/119
1B 910627	0.6329	34.6 ± 0.7	37.0 ± 0.7	−0.921 ± 0.021	−2.028 ± 0.018	124.51/104
1B 910629	0.1287	425.2 ± 26.9	167.9 ± 5.6	−0.507 ± 0.054	−1.940 ± 0.095	121.45/103
1B 910630	2.251×10^{-2}	257.1 ± 13.0	1145.3 ± 211.8	−1.426 ± 0.026	−5.000	98.91/100
1B 910709	4.541×10^{-3}	1229.6 ± 219.0	43.0 ± 0.9	1.978 ± 0.174	−1.634 ± 0.072	106.37/105
1B 910803	0.4254	306.3 ± 18.6	150.1 ± 5.6	−0.601 ± 0.069	−1.961 ± 0.105	111.74/103
1B 910809	0.4055	483.5 ± 37.1	621.1 ± 49.1	−1.026 ± 0.042	−5.000	99.93/103
1B 910814C	9.895×10^{-8}	423.3 ± 12.7	398.1 ± 10.3	−0.921 ± 0.018	−5.000	144.45/121
1B 910814B	3.306×10^{-6}	1643.2 ± 54.4	1275.4 ± 33.6	−0.876 ± 0.009	−5.000	128.86/101
1B 910905	2.359×10^{-2}	527.6 ± 20.9	127.0 ± 2.0	−0.308 ± 0.037	−1.750 ± 0.039	274.25/106
1B 910930	0.1673	110.9 ± 5.6	131.0 ± 7.5	−1.102 ± 0.070	−1.997 ± 0.090	124.14/103
1B 911016	2.810×10^{-24}	326.2 ± 6.9	87.8 ± 1.2	0.462 ± 0.045	−3.112 ± 0.340	108.80/102
1B 911031	0.1597	249.7 ± 5.5	364.7 ± 10.1	−1.123 ± 0.015	−2.116 ± 0.090	154.43/105
1B 911104	9.847×10^{-5}	409.5 ± 21.2	83.7 ± 1.8	−0.277 ± 0.053	−1.669 ± 0.034	121.18/115
1B 911106	1.860×10^{-13}	262.4 ± 5.5	97.5 ± 1.0	−0.264 ± 0.025	−2.174 ± 0.041	127.71/99
1B 911109	3.868×10^{-9}	181.2 ± 5.0	55.3 ± 0.8	0.057 ± 0.040	−2.144 ± 0.044	108.97/99
1B 911118	0	223.9 ± 2.0	90.7 ± 0.4	−0.169 ± 0.010	−2.718 ± 0.038	254.98/100
1B 911123	6.141×10^{-10}	95.1 ± 5.5	52.9 ± 1.4	−0.155 ± 0.070	−3.490 ± 0.652	84.11/105
1B 911126	2.430×10^{-5}	154.2 ± 2.3	352.8 ± 9.2	−1.309 ± 0.013	−2.017 ± 0.045	122.20/100
1B 911127	5.434×10^{-12}	128.4 ± 1.9	137.9 ± 1.8	−0.908 ± 0.022	−2.457 ± 0.067	118.32/103
1B 911202	2.560×10^{-2}	375.3 ± 6.9	540.5 ± 12.2	−1.108 ± 0.011	−2.158 ± 0.096	93.49/99
1B 911209	1.404×10^{-2}	224.0 ± 5.3	182.7 ± 3.4	−0.839 ± 0.027	−2.182 ± 0.073	97.05/102
1B 911210	3.489×10^{-4}	199.7 ± 17.2	121.1 ± 6.7	−0.399 ± 0.117	−5.000	91.13/102
1B 911217	3.303×10^{-3}	225.1 ± 16.8	61.0 ± 1.8	0.052 ± 0.087	−2.195 ± 0.137	122.97/102
1B 911227	1.893×10^{-2}	187.0 ± 6.3	130.2 ± 3.9	−0.910 ± 0.035	−1.782 ± 0.035	149.76/109
1B 920110	5.743×10^{-8}	311.5 ± 6.6	273.2 ± 4.6	−0.852 ± 0.018	−2.607 ± 0.165	119.76/107
1B 920130	7.184×10^{-16}	92.1 ± 7.0	41.7 ± 1.2	0.214 ± 0.040	−5.000	213.87/99
1B 920210	5.956×10^{-15}	812.1 ± 30.4	324.7 ± 6.5	−0.523 ± 0.019	−5.000	142.28/100
1B 920221	1.879×10^{-2}	95.6 ± 2.3	217.9 ± 7.8	−1.287 ± 0.017	−2.225 ± 0.098	125.40/109
1B 920226	2.734×10^{-3}	281.5 ± 10.2	100.5 ± 1.8	−0.358 ± 0.047	−1.929 ± 0.048	136.09/109
1B 920227	4.712×10^{-10}	262.5 ± 25.8	52.9 ± 1.3	0.725 ± 0.114	−3.244 ± 0.586	87.64/96
1B 920227B	3.115×10^{-4}	364.1 ± 19.9	203.3 ± 6.6	−0.649 ± 0.041	−2.558 ± 0.363	104.41/109
920307_01086	6.136×10^{-3}	177.6 ± 8.6	80.8 ± 2.0	−0.346 ± 0.066	−2.206 ± 0.106	119.20/96
920308_17747	8.393×10^{-2}	2845.5 ± 488.1	100000.0	−1.150 ± 0.028	−1.500	142.94/98
920311_08426	1.055×10^{-16}	448.4 ± 5.8	285.9 ± 2.7	−0.789 ± 0.008	−2.197 ± 0.041	139.10/101
920315_15569	0.5215	142.3 ± 6.8	137.0 ± 7.7	−1.087 ± 0.130	−1.864 ± 0.052	128.71/101
920320_44340	0.3836	73.9 ± 1.2	88.5 ± 1.5	−1.077 ± 0.015	−2.054 ± 0.029	138.17/102
920325_62257	8.598×10^{-2}	38.5 ± 0.5	13.0 ± 1.0	1.035 ± 0.020	−2.042 ± 0.020	162.37/107
920331_65750	2.178×10^{-6}	136.0 ± 4.0	93.3 ± 1.8	−0.663 ± 0.028	−2.534 ± 0.142	135.97/101
920404_47506	4.052×10^{-5}	266.8 ± 8.9	88.6 ± 1.5	−0.373 ± 0.039	−1.878 ± 0.037	87.88/98
920406_09855	1.731×10^{-17}	329.8 ± 3.4	212.7 ± 1.5	−0.718 ± 0.008	−2.326 ± 0.040	176.59/98
920502_62802	2.174×10^{-5}	231.8 ± 7.4	166.6 ± 3.7	−0.760 ± 0.028	−2.541 ± 0.191	117.31/101
920511_23247	0.3105	518.9 ± 67.3	639.6 ± 83.9	−1.023 ± 0.069	−5.000	107.32/100
920513_60781	3.536×10^{-18}	398.2 ± 9.0	120.3 ± 1.2	−0.311 ± 0.020	−2.028 ± 0.037	158.82/107
920517_11876	3.608×10^{-25}	395.3 ± 9.3	143.4 ± 1.6	−0.429 ± 0.017	−2.267 ± 0.058	120.89/107
920524_13904	0.3187	794.0 ± 61.0	608.1 ± 35.0	−0.876 ± 0.031	−3.251 ± 4.711	120.22/112
920525_12423	9.424×10^{-15}	564.7 ± 9.8	402.0 ± 5.1	−0.840 ± 0.008	−2.523 ± 0.137	122.27/103
920530_82797	0.9338	42.8 ± 2.9	38.6 ± 2.3	−0.858 ± 0.064	−2.040 ± 0.080	145.71/111

[a] Probability of the improvement in χ^2 if the simpler model ($\alpha = -1$ and $\beta = -2$ fixed) is correct.
[b] Break energy for the fits with $\alpha = -1$ and $\beta = -2$ fixed.
[c] Break energy for the fits with all parameters free to vary.
[d] Low-energy spectral index for the fits with all parameters free to vary.
[e] High-energy spectral index for the fits with all parameters free to vary.
[f] χ^2 and degrees of freedom for the fits with all parameters free to vary.
[g] Parameters without uncertainties were at the limits of the permitted range of values.

require a four-parameter fit, as the proportions in Table 5 show. This effect results from including a larger portion of the low-energy component in the spectrum, constraining the fit to model both the low- and high-energy power laws accurately. However, this is not a systematic effect which masks a universal spectrum, since there is a wide α-distribution with most values greater than $\alpha = -1$. Note that for all E_1 a four-parameter model is required for at least half the bursts. Figure 5 shows there is a large scatter in α at any given E_1, with no clear trend in the average α. Thus there is no evidence for a universal value of α.

The fits with all four parameters free to vary are generally statistically acceptable. Figure 6 compares the cumulative χ^2/ν distribution for the four-parameter model to the expected dis-

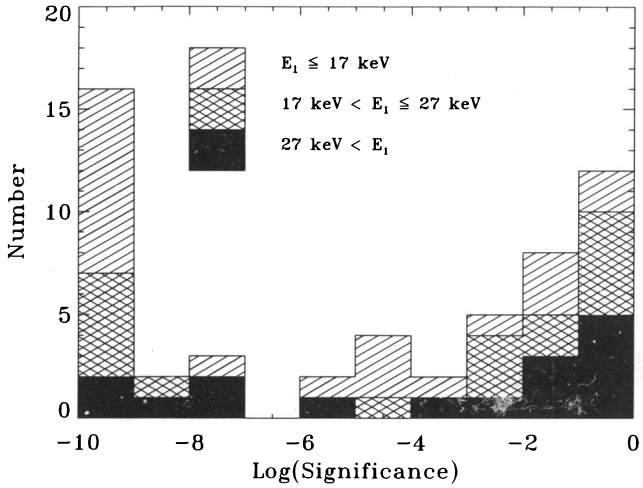

FIG. 4.—Distribution of bursts by the significance of the full four-parameter fit compared with a fit with fixed α and β. The significance is defined in the text; the smaller the significance, the less likely $\alpha = -1$ and $\beta = -2$. The histograms are also broken down by the low-energy cutoff of the fits. The bin between 10^{-10} and 10^{-9} actually contains all probabilities smaller than 10^{-9}.

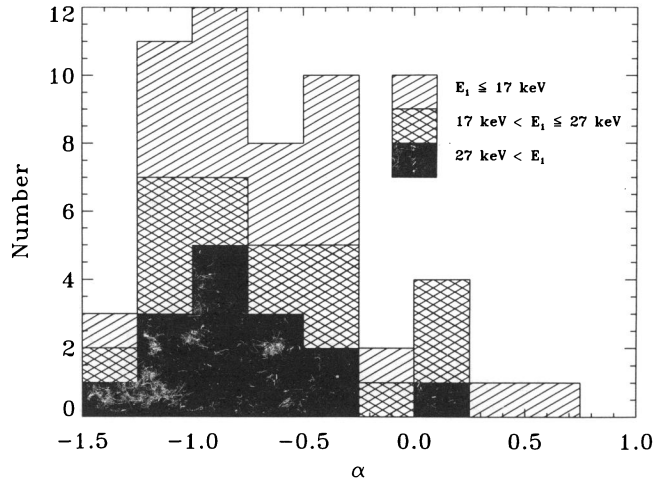

FIG. 5.—Distribution of α, the low-energy spectral index. The distributions are also broken down by the low-energy cutoff E_1 of the fitted spectrum.

tribution for 100 degrees of freedom (there is little difference in the theoretical distribution when the number of degrees of freedom differs by a few from 100). While the χ^2/ν distribution for the four-parameter fit is shifted to somewhat higher values than theoretically expected, the bulk of the χ^2/ν values lie close to unity. Formally this χ^2/ν distribution would indicate a poor fit, but in practice this distribution is reassuring. The small shift to larger χ^2/ν may be a consequence of underestimating the true uncertainties. For example, not included in the uncertainties are systematic effects such as the absence of Earth scatter in the detector response matrix and the low-energy inaccuracies of the calibration (see § 2.2).

For comparison, the cumulative χ^2/ν distribution for the two-parameter fits is also shown by Figure 6. As can be seen, the four-parameter fits are clearly superior as a class: the median $\chi^2/\nu = 1.20$ for the four-parameter fits, while $\chi^2/\nu = 1.47$ for the two-parameter fits. In our simulations we found that the average difference between χ^2/ν for a model with the true parameter values and the minimum found by CURFIT was 0.04, which is much smaller than the difference between the two- and four-parameter fits. The two distributions are different with a significance of 5×10^{-3} by the Kolmogorov-Smirnov test. Finally, note that the two-parameter fit distribution has a tail to large values of χ^2/ν.

For completeness we note that as the spectral resolution increases with successive instruments, the continuum will be characterized more accurately. While our four-parameter model appears to be sufficient to describe the burst continuum observed by BATSE, more accurate instruments will probably require a more sophisticated model in the future. Indeed, the BATSE spectra hint that different spectral models will be required in the future, since we find that the break energy E_0 sometimes increases as the energy range of the fit is shifted to higher energies, suggesting that the model accommodates the true spectrum which curves continuously over the observed energy range. However, note that a comparison of the observed spectra and the fitted models reveals no systematic deviations. We also do not find any dependence of χ^2/ν on the fluence (see the discussion on fluences below), a measure of the signal-to-noise ratio. Since we showed in § 3 that an overly simplified model will give acceptable χ^2/ν for small S/N, but will become unacceptable as the quality of the spectrum improves, this indicates that the four-parameter model is a good approximation to the shape of the BATSE spectra.

Figure 7 plots α versus β. It should be noted that α was constrained in our fits to fall between -1.5 and 2, and β between -5 and -1.5. There does not appear to be a clear relationship between α and β, and indeed we find that the

TABLE 5

SIGNIFICANCE OF FOUR-PARAMETER FIT, BY LOW-ENERGY CUTOFF E_1

E_1 (keV)	$P < 10^{-2}$	$10^{-2} < P < 10^{-1}$	$10^{-1} < P$
7–17.....	0.7619 (16)	0.1429 (3)	0.0952 (2)
17–27.....	0.5882 (10)	0.1176 (2)	0.2941 (5)
27–37.....	0.5 (8)	0.1875 (3)	0.3125 (5)

NOTE.—The number of bursts in each category is given in parentheses.

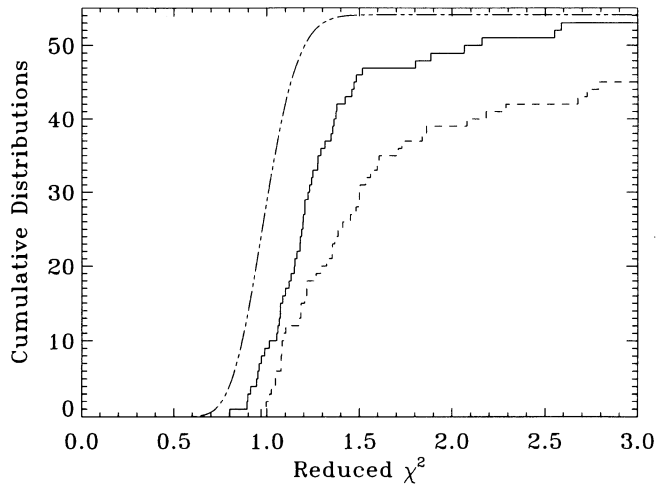

FIG. 6.—Cumulative reduced χ^2 distribution. The solid curve corresponds to the fits with all four parameters free to vary, while α and β were fixed for the fits shown by the dashed curve. The dot-dot-dash curve shows the ideal χ^2/ν for 100 degrees of freedom, normalized to the number of bursts.

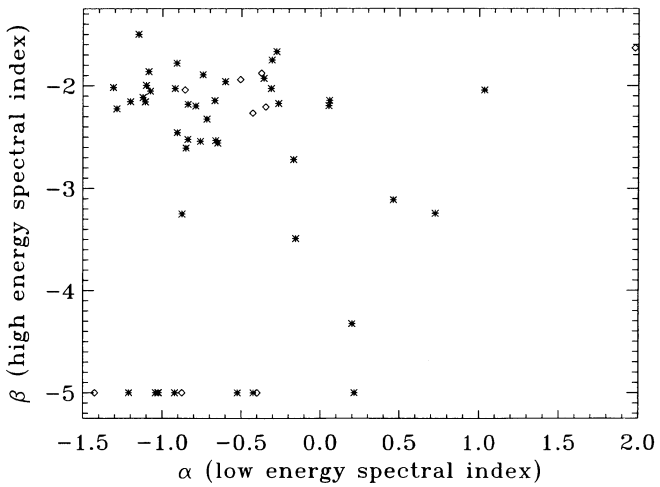

FIG. 7.—Plot of β vs. α. Uncertainties have been suppressed for display purposes but are typically ~ 0.05 for α and ~ 0.25 for β. The points are coded by morphological class: complex (*asterisks*) and single (*diamonds*).

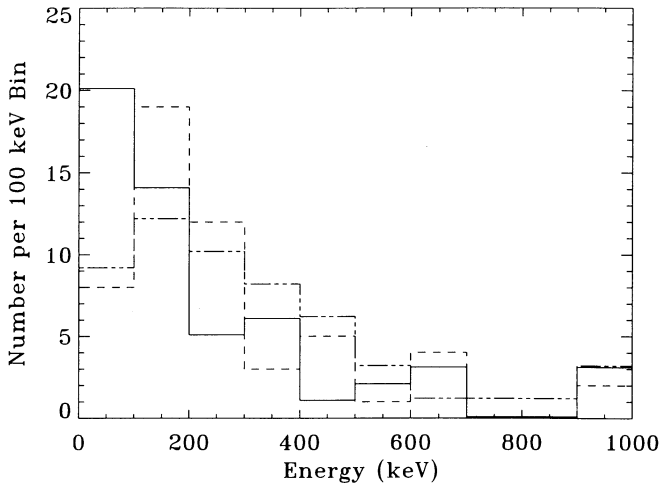

FIG. 8.—Distribution of E_0 from fits with all four parameters free to vary (*solid curve*) and from fits with $\alpha = -1$ and $\beta = -2$ (*dot-dot-dash curve*). Also shown is the distribution of "hardness," the peak of $E^2N_E(E)$ (*dashed curve*).

linear correlation coefficient is nearly zero. However, the spectral indices populate a particular part of parameter space: β is typically found between -2 and -2.5 when it can be determined, and α is between 0 and -1.5. The spread in β-values appears to be a little smaller than the spread in α. It should be noted that the uncertainty in α (0.044) is smaller than in β (0.219 excluding those bursts for which β hit the range constraints).

An interesting question is whether those bursts with $\beta \sim -5$ (11 bursts where the fit hit the constraint $\beta \geq -5$, and one with $\beta = -4.3$) really do not have a high-energy tail, or whether the small number of high-energy counts makes it difficult to observe such a tail. Assuming $\beta = -2$ on average, the high-energy tail is not evident until $(\alpha + 2)E_0$. Thus the ratio of $(\alpha + 2)E_0$ to $E_{3\sigma}$ is a measure of how well the high-energy power law can be determined. We find that for nine of the 12 bursts with $\beta < -4$ this ratio is greater than the average ratio for the remaining bursts (i.e., those with $\beta > -4$), and for three of these bursts with $\beta < -4$ the ratio is of order unity. As we showed in § 3, spectra with poor S/N will be fitted by the correct parameter values on average, but with a large dispersion. Thus, the spectra with $\beta < -4$ are part of the population with few high S/N channels in the high-energy tail, and consequently are fitted by a wide β-distribution. This is supported by additional SD data: as noted in § 2.2, the SDs usually provided more than one spectrum of each burst. Of the eight bursts with $\beta = -5$ and at least one spectrum extending to high energy (from a low gain detector), three had $\beta > -5$ in a joint fit to the high- and low-energy spectra. For one of the three remaining bursts with $\beta = -5$, a fit to a second low-energy spectrum (from a high-gain detector) gave $\beta > -5$. Finally, the absence of a high-energy tail may result from a systematic data analysis error such as an incorrectly large interpolated background spectrum. The background has approximately an $E^{-1.5}$ dependence and thus dominates the steeper high-energy burst spectra. Consequently, the background-substracted burst spectrum is particularly sensitive to errors in the background at high energies. For these many reasons the absence of an observed high-energy tail (i.e., a component flatter than an exponential) may be an observational artifact, although we cannot rule out the possibility that the high-energy spectrum for these events may be truly soft.

Both the two- and four-parameter fits result in a wide distribution of E_0; as shown in Figure 8, there is no universal value of E_0. The distribution for the two-parameter fit does indeed peak around $E_0 = 150$ keV, but extends to much higher values. Freeing α to vary generally results in low values of E_0 (compared with the two-parameter fit), since an increase in α compensates for a decrease in E_0. Indeed, the lower values of E_0 in the four-parameter fits compared with the two-parameter fits all occur for $\alpha > -1$.

The hardness of the two-parameter fit can be characterized by E_0, the only quantity which can change the spectral shape. Because the four-parameter fit has three varying quantities which change the shape, E_0 is an inadequate hardness measure for these fits. We therefore define the hardness as the maximum in $E^2N(E)$, which is proportional to νF_ν used in other astronomical subfields. The quantity $E^2N(E)$ is the energy flux per logarithmic energy band; its maximum indicates the energy band where most of the energy is radiated. For a power law with $\beta > -2$, $E^2N(E)$ peaks at the power law's high-energy cutoff, which cannot be determined from our spectra, while for $\beta < -2$ the peak is at the lower end of the power law. Further, β generally has large uncertainties. Consequently, we calculate the maximum of $E^2N(E)$ from the low-energy component alone, ignoring the high-energy power law. Thus we define the hardness as $H = (2 + \alpha)E_0$. Note that by this definition E_0 is indeed the hardness for $\alpha = -1$. The hardnesses from the four-parameter fits are listed in Table 6 and shown in Figure 8.

In Table 6 we also present $S_{\rm Kon}$, the fluence calculated over the energy range 30–2000 keV and meant to correspond to the Konus fluences, and S_{SMM}, calculated over 0.3–10 MeV and thus comparable to *SMM* fluences. In many cases the integral over the model spectrum was dominated by energies outside the energy range fitted; consequently, these fluences are by no means the definitive values for these bursts.

4.2. *Test of Cosmological Model*

Bursts at cosmological distance will undergo relativistic effects which may be apparent in correlations among the hardness, burst duration, fluence, and peak photon flux: time dilation increases the burst duration, while the redshift downshifts the spectrum (Paczyński 1991, 1992; Dermer 1992). In brief, we expect harder bursts to be shorter, brighter (greater peak

TABLE 6

BURST HARDNESS AND FLUENCES

Burst	Hardness (keV)	S_{Kon} (ergs cm^{-2}) (0.03–2 MeV)	S_{SMM} (ergs cm^{-2}) (0.3–10 MeV)
1B 910430	246.6 ± 12.4	1.757×10^{-5}	6.163×10^{-6}
1B 910502	11.8 ± 0.2	1.615×10^{-5}	9.886×10^{-6}
1B 910503	465.8 ± 4.3	1.178×10^{-4}	1.285×10^{-4}
1B 910507	158.2 ± 5.6	5.568×10^{-6}	7.915×10^{-7}
1B 910511	128.6 ± 14.5	2.038×10^{-6}	2.219×10^{-6}
1B 910523	76.7 ± 9.2	4.923×10^{-7}	1.092×10^{-8}
1B 910601	574.7 ± 15.4	7.567×10^{-5}	4.909×10^{-5}
1B 910627	39.9 ± 1.1	1.886×10^{-5}	1.492×10^{-5}
1B 910629	250.7 ± 12.3	6.449×10^{-6}	7.446×10^{-6}
1B 910630	657.4 ± 125.3	1.051×10^{-5}	7.047×10^{-6}
1B 910709	170.9 ± 8.2	2.147×10^{-6}	4.002×10^{-6}
1B 910803	210.0 ± 13.0	8.879×10^{-6}	9.500×10^{-6}
1B 910809	605.0 ± 54.3	6.375×10^{-6}	4.269×10^{-6}
1B 910814C	429.5 ± 13.1	3.739×10^{-4}	2.056×10^{-4}
1B 910814B	1433.9 ± 39.5	1.033×10^{-4}	1.172×10^{-4}
1B 910905	214.9 ± 5.8	3.566×10^{-5}	5.325×10^{-5}
1B 910930	117.6 ± 11.3	6.531×10^{-6}	5.809×10^{-6}
1B 911016	216.3 ± 5.0	1.054×10^{-5}	4.159×10^{-6}
1B 911031	319.8 ± 10.4	3.162×10^{-5}	2.878×10^{-5}
1B 911104	144.2 ± 5.4	9.518×10^{-6}	1.547×10^{-5}
1B 911106	169.3 ± 2.9	2.472×10^{-5}	1.918×10^{-5}
1B 911109	113.7 ± 2.8	9.208×10^{-6}	6.781×10^{-6}
1B 911118	166.0 ± 1.1	6.500×10^{-5}	2.638×10^{-5}
1B 911123	97.7 ± 4.5	1.600×10^{-6}	1.764×10^{-7}
1B 911126	243.8 ± 7.8	5.558×10^{-5}	5.187×10^{-5}
1B 911127	150.6 ± 3.6	2.630×10^{-5}	1.285×10^{-5}
1B 911202	482.1 ± 12.4	4.975×10^{-5}	4.935×10^{-5}
1B 911209	212.1 ± 6.3	2.371×10^{-5}	1.850×10^{-5}
1B 911210	193.9 ± 17.7	1.715×10^{-6}	3.784×10^{-7}
1B 911217	125.2 ± 6.4	2.799×10^{-6}	1.956×10^{-6}
1B 911227	142.0 ± 6.3	1.550×10^{-5}	2.031×10^{-5}
1B 920110	313.7 ± 7.1	4.016×10^{-5}	2.554×10^{-5}
1B 920130	92.3 ± 3.1	1.058×10^{-5}	2.839×10^{-7}
1B 920210	479.6 ± 11.4	3.953×10^{-5}	2.461×10^{-5}
1B 920221	155.4 ± 6.8	9.792×10^{-6}	6.331×10^{-6}
1B 920226	165.0 ± 5.6	2.025×10^{-5}	2.208×10^{-5}
1B 920227	144.1 ± 7.0	8.641×10^{-7}	1.946×10^{-7}
1B 920227B	274.6 ± 12.2	1.135×10^{-5}	7.078×10^{-6}
920307_01086	133.6 ± 6.2	7.008×10^{-6}	4.803×10^{-6}
920308_17747	2077.2 ± 67.2	1.401×10^{-5}	3.293×10^{-5}
920311_08426	346.2 ± 3.9	1.091×10^{-4}	9.996×10^{-5}
920315_15569	125.1 ± 19.1	1.176×10^{-5}	1.319×10^{-5}
920320_44340	81.7 ± 1.9	2.456×10^{-5}	1.911×10^{-5}
920325_62257	39.3 ± 3.0	2.602×10^{-5}	2.006×10^{-5}
920331_65750	124.8 ± 3.6	2.127×10^{-5}	8.776×10^{-6}
920404_47506	144.1 ± 4.2	1.083×10^{-5}	1.249×10^{-5}
920406_09855	272.7 ± 2.6	9.604×10^{-5}	7.160×10^{-5}
920502_62802	206.6 ± 6.5	1.272×10^{-5}	6.726×10^{-6}
920511_23247	624.9 ± 93.2	9.380×10^{-6}	6.399×10^{-6}
920513_60781	203.2 ± 3.0	4.598×10^{-5}	4.567×10^{-5}
920517_11876	225.3 ± 3.5	2.301×10^{-5}	1.738×10^{-5}
920524_13904	683.5 ± 43.6	2.482×10^{-5}	1.998×10^{-5}
920525_12423	466.4 ± 6.8	8.348×10^{-5}	6.864×10^{-5}
920530_82797	44.1 ± 3.6	1.984×10^{-6}	1.536×10^{-6}

photon flux), and more energetic (larger fluence). However, a large range of intrinsic luminosities, durations, and spectral shapes will obscure the cosmological signature, as will evolution in the intrinsic burst properties. In addition, the peak count rate criterion used to construct the sample biases the correlations (Schaefer 1993); for example, hard bursts have fewer counts than soft bursts at a given fluence, and thus must have a higher fluence to be included in the sample. Finally, by including only the bright bursts which are preferentially nearby, we may not find a strong cosmological effect, even though the $\sim P^{-0.8}$ dependence of our sample's cumulative peak flux distribution suggests that our bursts are not spatially homogeneous (§ 2.3).

Table 7 summarizes the correlations of the fluence, peak flux, and duration with hardness. For cosmological bursts we expect the hardness to be correlated with the fluence and peak flux, and anticorrelated with the burst duration. The fluence S_{BAT} (above 20 keV), peak flux P_{BAT} (50–300 keV) on a 64 ms time scale, and burst duration Δt are from LAD observations; for bursts before 1992 February these quantities can be found in the First BATSE Burst Catalog (Fishman et al. 1993), while preliminary unpublished values were used for subsequent bursts. The two fluences S_{Kon} and S_{SMM} were calculated from our fits and can be found in Table 6. In addition to the correlation parameters a and b and coefficient r, we include in Table 7 $P(>|r|)$, the probability of a spurious correlation. We consider $P(>|r|) \sim 10^{-2.5}$ or smaller to be significant. As can be seen from Table 7, we find significant correlations, but these do not fulfill the predictions of the cosmological models; these correlations may indicate trends intrinsic to the burst process (e.g., longer bursts are harder).

4.3. *Search for Other Correlations*

The bursts observed by BATSE do not show any spatial anisotropies (Meegan et al. 1992), nor do subsamples based on intensity or morphology. However, subpopulations based on different criteria may be anisotropic. Therefore, we compared the hardness distributions of the following spatial subsamples: toward the Galactic plane ($|b| < 30°$) compared with toward the Galactic pole ($|b| > 30°$); north ($b > 0°$) and south ($b < 0°$) Galactic hemispheres; north and south equatorial hemispheres (declination greater than and less than 0°); toward and away from the Galactic center ($l < 90°$ or $l > 270°$ compared with $90° < l < 270°$); and, finally, right ascension less than and greater than 12^h. In some cases the comparison was qualitatively tantalizing, yet in no case was any set of subsamples different by the Kolomogorov-Smirnov test. Specifically, the probability that the two subsamples were drawn from the same population was large for all comparisons (the smallest probability was 0.235).

Unfortunately, our sample consists predominantly of

TABLE 7

CORRELATION BETWEEN BURST PROPERTIES AND SPECTRAL HARDNESS

X	Y	a	b	r	$P(>\|r\|)$
$\log_{10}(S_{BAT})$	$\log_{10} H$	3.572	0.250	0.408	2.424×10^{-3}
$\log_{10}(S_{Kon})$	$\log_{10} H$	3.573	0.263	0.395	3.119×10^{-3}
$\log_{10}(S_{SMM})$	$\log_{10} H$	3.312	0.201	0.417	1.710×10^{-3}
$\log_{10}(P_{BAT})$	$\log_{10} H$	2.380	-7.666×10^{-2}	-8.049×10^{-2}	0.567
$\log_{10}(\Delta t)$	$\log_{10} H$	2.065	0.299	0.426	1.471×10^{-3}

NOTE.—The linear fit was $Y = a + bX$, and r is the linear correlation coefficient.

complex, multipeak bursts, with only nine of the 54 bursts possessing different morphologies. These nine events do not populate a different part of parameter space although three of the nine have $\beta = -5$, and thus do not show a high-energy tail in our fits. However, we are dealing with only a small number of bursts, and cannot draw significant conclusions.

4.4. *High-Energy Breaks*

In an earlier study (Schaefer et al. 1992, hereafter S92), we fitted spectra from a sample of bursts observed by the BATSE SDs, but over the energy range 100 or 300 keV to ~27 MeV. Five bursts in S92 were found to require a break in the model spectrum: a broken power law gave a better fit than a simple power law. The resulting breaks were interpreted as possibly reflecting an underlying emission mechanism tied to the electron rest mass, such as photon–magnetic field or photon-photon pair opacity, or the rolloff in the Klein-Nishina cross section. The spectral analysis by S92 is consistent with the fits presented here, although we suspect that the implications regarding the emission mechanism are not as interesting.

We suspect that in S92 we did not find a larger number of spectral breaks, or breaks below 400 keV, because in that study we fitted our spectra above 100 keV, whereas here our spectra extend below ~30 keV. Thus, in the current survey we include the soft low-energy part of the spectrum, requiring a spectral break which is usually below 400 keV. Note that here we did not test the hypothesis that a simple power law could be rejected. However, in most cases we find a significant spectral break: $\alpha - \beta$ is less than 0.5 for only one burst, less than 0.75 for only two, and less than 1 for nine of the 54 bursts in the sample (the conclusions are the same even when the uncertainties are considered).

In the current fits we find that $\beta = -5$ for four of the five bursts that show curvature in our S92 sample. The break energies we found in S92 and here are qualitatively the same for each of the four bursts; given the difference in spectral models and energy range, quantitative agreement is not expected (in S92 our model was a broken power law with a sharp break). The fifth burst with a break found in S92 is 1B 910503, the strong burst also observed by two other *GRO* experiments (Schneid et al. 1992; Winkler et al. 1992). In our new fit for this burst we find that the spectrum breaks at half the energy we reported in S92, and the power law above the break is harder. This is a consequence of the energy ranges over which the spectra were fitted in our two studies. When the spectrum from the high-gain detector 6 (in S92 we used the low-gain detector 4, which covered a higher energy range) is fitted from 300 to 3000 keV, the break energy E_0 doubles compared with the value given by a fit over the range 30–3000 keV. As discussed in § 4.1, the true continuum is most likely a continuously curving spectrum below a few hundred keV which is approximated sufficiently well by the GRB function (eq. [1]) we used here or by the broken power law we used in S92; consequently, as the energy range is shifted higher, the break energy increases. Nonetheless, the significant curvature appears to be at low energy.

Therefore, we conclude that the high-energy breaks we found in S92 are the tail of the distribution of breaks; a greater number of lower energy breaks were not detected because the fits in S92 did not extend below 100 keV. In addition, the break energies in both S92 and the current study may be biased by the energy range over which the spectra were fitted, and spectra should be compared over similar energy ranges.

5. DISCUSSION

The spectra presented in this work were accumulated over entire bursts. Since bursts show significant spectral evolution, the great spectral diversity we find results not just from differences in the instantaneous spectrum but also from temporal variations. Thus, we are seeing variety between bursts not only in the emitting regions but also in the evolution of these regions. To separate properly the spectral and temporal signatures requires a study of the spectral evolution, which will be the subject of a future investigation (Band et al. 1993b). Nonetheless, the present study shows that there is not a universal average burst spectrum, even though a simple four-parameter function adequately describes the diverse spectra.

Because the current emission theories are not very constraining, the spectral diversity we demonstrated is not much more difficult for these theories to explain than a single universal spectrum. In particular, the theories often attribute the spectral parameters to unknown physics (e.g., particle acceleration). For example, the Galactic neutron star model of Dermer (1990) and Vitello & Dermer (1991) finds that the spectral index of the high-energy tail is the same as the injected electron distribution, and the break between the low- and high-energy power laws is proportional to the product of the magnetic field and the electron distribution's low-energy cutoff. Furthermore, the low-energy component varies between $\alpha = 0$ and -1, depending on conditions within the emitting region. Thus, changing the injected electron distribution or varying the magnetic field between burst sources can provide the necessary variety.

No successful burst spectrum has yet been calculated for the cosmological models, and thus it is not known whether spectral diversity is a difficulty for these models. The original fireball models (Goodman 1986; Paczyński 1986) resulted in spectra which are closer to blackbodies than to gamma-ray burst spectra. However, as Paczyński (1991) points out, the collision of two compact bodies, such as a neutron star and a Kerr black hole, has sufficient free parameters to explain the diversity of burst phenomena such as duration, morphology, and spectrum.

The turnover in the spectrum, represented by E_0 or the hardness H, has been tied to fundamental physical processes such as pair creation (e.g., Harding 1991; S92; Baring 1992). Yet the broad distribution of turnover energies is striking (Fig. 8). In addition, the distribution peaks far below characteristic energies such as 511 keV and shows no features at such energies; Konus found a similar distribution of turnover energies (Mazets et al. 1982). This broad distribution may indicate that a wide range of conditions—magnetic fields, densities, acceleration processes—exist in burst emission regions. This is consistent with the strong spectral evolution seen in a number of bursts (Norris et al. 1986; Band et al. 1992): there is a distribution of turnover energies not only between bursts but also within bursts. The absence of observed features around 511 keV may indicate that the spectrum is sculpted by a complex series of physical processes such as evolving electron distributions and varying magnetic fields, as opposed to processes tied to specific fundamental energies such as the electron rest mass (e.g., photon-photon or photon–magnetic field pair opacity) or an atomic or nuclear line. Pair cascades may be important in the evolution of the radiating particle distributions but do not leave an unambiguous signature on the continuum. Also, this does not preclude pair processes occasionally producing an observable feature, but such features are not present through-

out an entire burst. If bursts originate at cosmological distances, their spectra will be redshifted, and features produced by pair processes will be observed at a variety of lower energies. By this hypothesis bursts with low break energies were produced at higher redshift than bursts with high break energies.

We did not find the correlations between spectral hardness and duration, fluence, or peak flux predicted by the cosmological models of burst origin. However, our burst sample may not have been complete, large, deep, or unbiased enough (§ 4.2), and thus we do not find the absence of a cosmological signature to be conclusive . These correlations may be indicative of intrinsic burst properties.

6. SUMMARY

We analyzed the spectra of 54 bursts averaged over the entire burst. Accumulated by the BATSE spectroscopy detectors on *GRO*, the spectra cover the energy range beginning at $\sim$10–30 keV and ending at $\sim$1300–3000 keV in 256 pseudologarithmic channels. The spectra were modeled successfully by the spectral form $N_E \propto E^{\alpha} \exp(-E/E_0)$ at low energies and $N_E \propto E^{\beta}$ at high energies. However, we find a distribution of values of α, β, and E_0, and not the universal values early studies found, such as $\alpha = -1$, $\beta = -2$, or $E_0 = 150$ keV.

The turnover in the spectrum occurs over a wide range of energies ranging from less than 50 keV to more than 1 MeV, whether the turnover is considered to be the spectral break energy E_0 or the hardness [defined as the maximum of $E^2N_E(E)$]. The distribution of turnover energies peaks below 200 keV, with few values above 400 keV. Therefore, it is unlikely that the turnover in most bursts is produced directly by pair processes (e.g., pair-production opacity) unless the burst souces are distributed over a wide redshift range.

The cosmological model predicts that fainter bursts should be softer and longer as a consequence of the cosmological redshift and time dilation. Although we do find correlations of the hardness with the burst fluence and duration, they do not agree with the cosmological prediction. However, our sample was probably not appropriate for such a study, and consequently we cannot make a definitive statement about the cosmological model. The correlations we did find may reveal fundamental burst properties, such as that longer bursts are harder.

We also searched for, but did not find, a correlation between spectral hardness and the spatial distribution. Our sample consists predominantly of complex bursts with few simple, short-duration bursts. In a higher fraction of the simpler bursts no high-energy tail was found, but otherwise there are no striking spectral differences based on temporal morphology.

Finally, we studied the dependence of the fitting process on particulars of the SD data. Low S/N observed spectra with a high-energy tail can be fitted by statistically acceptable models without a high-energy component; the resulting fitted low-energy component will be harder than the true underlying spectrum. Consequently, high-energy tails should be included in the fits to all spectra even if not justified statistically, because their existence has been demonstrated in spectra of intense bursts.

Future studies will focus on spectral evolution during a burst.

We thank D. Gruber, R. Lingenfelter, and R. Rothschild for stimulating discussions on GRB spectra. This work was supported in part by NASA contract NAS8-36081 (UCSD group).

REFERENCES

Band, D. L., et al. 1992, in AIP Conf. Proc. 265, Gamma-Ray Bursts, ed. W. S. Paciesas & G. J. Fishman (New York:AIP), 169
Band, D. L., et al. 1993a, Exp. Astron. 2, 307
Band, D. L., et al. 1993b, in preparation
Barat, C., Chambon, G., Hurley, K., Niel, M., Vedrenne, G., Estulin, I. V., Kuznetsov, A. V., & Zenchenko, V. M. 1981, Ap&SS, 75, 83
Barat, C., Hurley, K., Niel, M., Vedrenne, G., Mitrofanov, I. G., Estulin, I. V., Zenchenko, V. M., & Dolidze, V. Sh. 1984, ApJ, 286, L11
Baring, M. G. 1992, Nature, 358, 624
Bevington, P. R. 1969, Data Reduction and Error Analysis for the Physical Sciences, (New York: McGraw-Hill)
Briggs, M. 1991, Ph.D. thesis, Univ. California at San Diego
Cline, T. L., & Desai, U. D. 1975, ApJ, 196, L43
Cline, T. L., Desai, U. D., Klebesadel, R. W., & Strong, I. B. 1973, ApJ, 185, L1
Dermer, C. D. 1990, ApJ, 360, 197
Dermer, C. D. 1992, Phys. Rev. Lett., 68, 1799
Eadie, W. T., Drijard, D., James, F. E., Roos, M., & Sadoulet, B. 1971, Statistical Methods in Experimental Physics (Amsterdam: North-Holland)
Fishman, G. J., et al. 1989a, in Proc. *Gamma Ray Observatory* Science Workshop (Washington: NASA), 2–39
———. 1989b, in Proc. *Gamma Ray Observatory* Science Workshop (Washington: NASA), 3-47
———. 1993, in preparation
Goodman, J. 1986, ApJ, 308, L47
Harding, A. K. 1991, Phys. Rep., 206, 327
Higdon, J. C., & Lingenfelter, R. E. 1990, ARA&A, 28, 401
Hurley, K. 1989, in NATO ASI Series C, Vol. 270, Cosmic Gamma Rays, Neutrinos, and Related Astrophysics, ed. M. M. Shapiro & J. P. Wefel (Dordrecht: Kluwer), 337
Kouveliotou, C., Paciesas, W. S., Fishman, G. J., Meegan, C. A., & Wilson, R. B. 1992, in The Compton Observatory Science Workshop ed. C. Scrader, N. Gehrels, & B. Dennis (NASA CP-3137), 61
Martin, B. R. 1971, Statistics for Physicists (London: Academic)
Matz, S. M., Forrest, D. J., Vestrand, W. T., Chupp, E. L., Share, G. H., & Rieger, E. 1985, ApJ, 288, L37
Mazets, E. P., et al. 1982, Ap&SS, 82, 261
Meegan, C. A., Fishman, G. J., Wilson, R. B., Paciesas, W. S., Pendleton, G. N., Horack, J. M., Brock, M. N., & Kouveliotou, C. 1992, Nature, 355, 143
Norris, J. P., Share, G. H., Messina, D. C., Dennis, B. R., Desai, U. D., Cline, T. L., Matz, S. M., & Chupp, E. L. 1986, ApJ, 301, 213
Paczyński, B. 1986, ApJ, 308, L43
———. 1991, Acta Astron., 41, 257
———. 1992, Nature, 355, 521
Pendleton, G. N., Paciesas, W. S., Lestrade, J. P., Fishman, G. J., Wilson, R. B., & Meegan, C. A. 1989, in Proc. *Gamma Ray Observatory* Science Workshop (Washington: NASA), 4-547
Schaefer, B. E. 1991, BATSE Spectral Analysis Software: User's Guide
———. 1993, ApJ, 404, L87
Schaefer, B. E., et al. 1992, ApJ, 393, L51 (S92)
Schneid, E. J., et al. 1992, A&A, 255, L13
Vitello, P., & Dermer, C. D. 1991, ApJ, 374, 668
Winkler, C., et al. 1992, A&A, 255, L9